

A New Spin-Correlated Plasmon in Novel Highly Oriented Single-Crystalline Gold Quantum Dots

Bin Leong Ong, Muhammad Avicenna Naradipa, Angga Dito Fauzi, Muhammad Aziz Majidi, Caozheng Diao, Satoshi Kurumi, Pranab Kumar Das, Chi Xiao, Ping Yang, Mark B. H. Breese, Sheau Wei Ong, Khay Ming Tan, Eng Soon Tok, and Andriyo Rusydi*



Cite This: *Nano Lett.* 2021, 21, 7448–7456



Read Online

ACCESS |

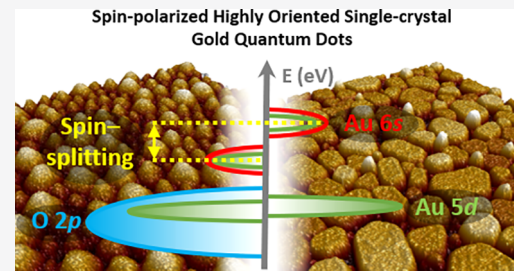
Metrics & More

Article Recommendations

Supporting Information

ABSTRACT: A concept of spin plasmon, a collective mode of spin-density, in strongly correlated electron systems has been proposed since the 1930s. It is expected to bridge between spintronics and plasmonics by strongly confining the photon energy in the subwavelength scale within single magnetic-domain to enable further miniaturizing devices. However, spin plasmon in strongly correlated electron systems is yet to be realized. Herein, we present a new spin correlated-plasmon at room temperature in novel Mott-like insulating highly oriented single-crystalline gold quantum-dots (HOSG-QDs). Interestingly, the spin correlated-plasmon is tunable from the infrared to visible, accompanied by spectral weight transfer yielding a large quantum absorption midgap state, disappearance of low-energy Drude response, and transparency. Supported with theoretical calculations, it occurs due to an interplay of surprisingly strong electron–electron correlations, s–p hybridization and quantum confinement in the s band. The first demonstration of the high sensitivity of spin correlated-plasmon in surface-enhanced Raman spectroscopy is also presented.

KEYWORDS: gold, highly oriented, self-organized, quantum-dots, quantum-confinement, electron-correlation, spin-polarization



INTRODUCTION

Many-body electronic correlations and spectral weight transfer play important roles in driving exotic phenomena such as high-temperature superconductivity, colossal magneto resistivity, and metal–insulator transition in strongly correlated electron systems. An exotic but less-explored phenomenon is a spin plasmon, a quasiparticle due to a quantum oscillation of spin density in strongly correlated electron systems proposed by Sir Mott in 1936.^{1,2} The spin plasmon is important for both new fundamental science and would open entirely novel future applications. For instance, it is expected to bridge between spintronics and plasmonics and, consequently, spin-photon interaction may occur in such a small-scale of magnetic domain and is therefore much faster and more energy-efficient than the electron-photon interaction. The spin-plasmonics, thus, plays an important role in shaping the future of fast low-energy high-density data transfer. While spin plasmon in a strongly correlated electron system remains to be realized, its relationship between electronic correlations and quantum confinement such as dimensionalities is rarely explored.

Unlike conventional plasmons in metals where long-range Coulomb interactions are dominating,^{3–6} many-body electronic correlations, that is, an interplay between short-(local) and long-range interactions,⁷ play important roles in determining spin correlated-plasmons in Mott-like insulators. The fingerprint of electronic correlations is essentially spectral weight transfer in a broad energy range as a function of

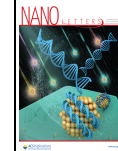
electron- or hole-doping, or temperature.^{1,8–11} Recently, an unconventional form of charge plasmons in a Mott-like insulator^{1,8} has been found in strongly correlated oxide $\text{Sr}_{1-x}\text{Nb}_{1-y}\text{O}_{3+\delta}$ as a manifestation of charge correlated-plasmons.¹² Unlike the conventional charge plasmons in metals, these plasmons did not originate from collective excitations of free charges. Instead, they arose from correlated electrons due to nanometer-spaced confinement and oxygen, which enhanced unscreened Coulomb interactions. In this Communication, we present a path to generate a new spin plasmon in s band of novel Mott-insulator gold and to demonstrate the first application of spin correlated-plasmons in surface-enhanced Raman spectroscopy (Spin-SERS).

Gold (Au) [$\text{Xe} 4f^{14} 5d^{10} 6s^1$] is a noble metal with diverse applications in society.¹³ From the discovery of the atomic nucleus to decorative jewelry, luxury goods, and medicine, its conducting properties make it useful for many modern technological platforms including microelectronics, energy-harvesting, lighting, and displays. Quantum confinement

Received: December 19, 2020

Revised: August 25, 2021

Published: September 9, 2021



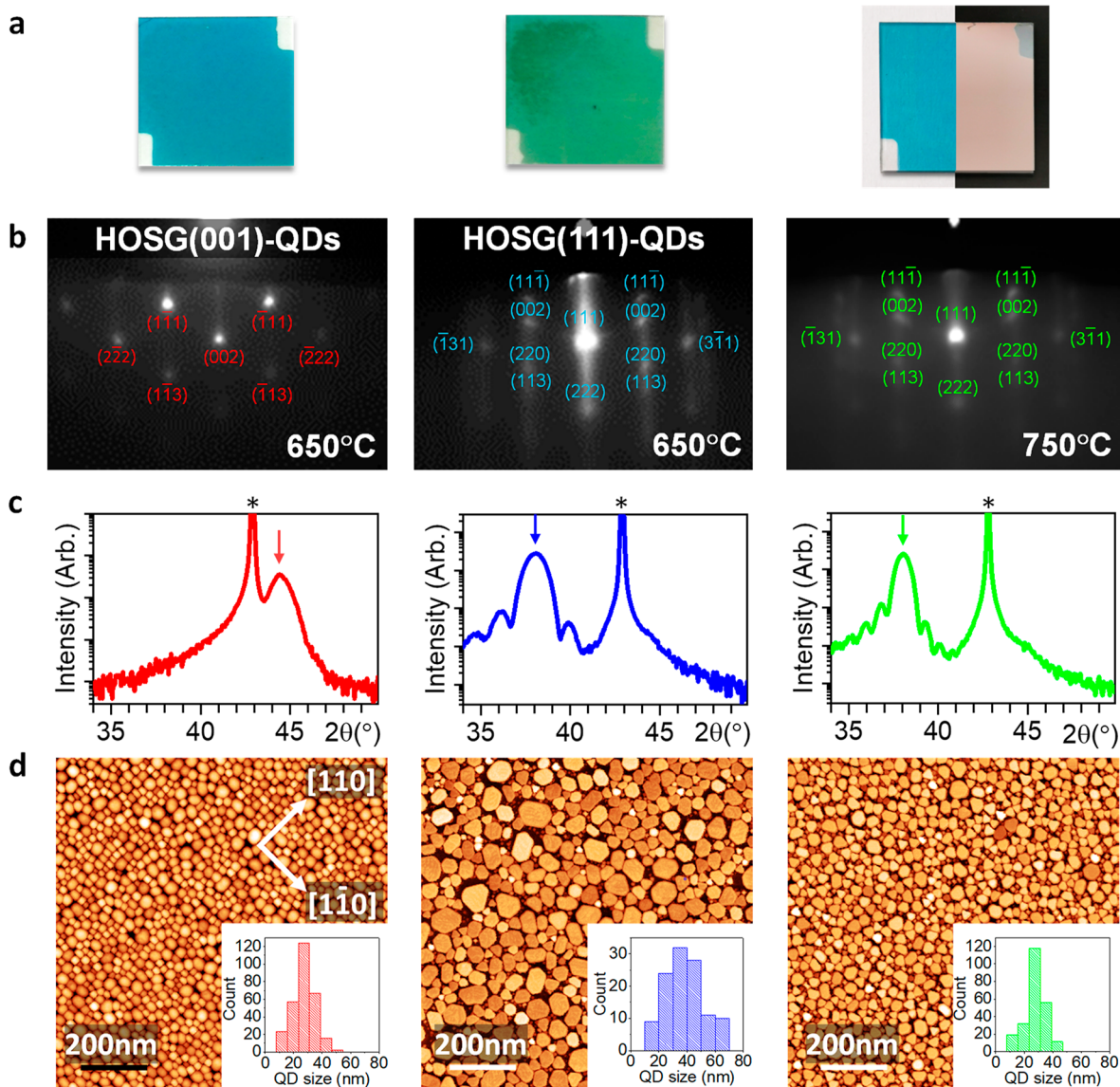


Figure 1. Control of HOSG-QDs growth and orientation on MgO(001) using UHV-MBE-PLD. HOSG(001)-QDs and HOSG(111)-QDs are formed with and without O₂ overpressure, respectively, when grown above 300 °C. (a) Transparency and change of color of HOSG-QDs when viewed against white and black backgrounds. (b) Real-time *in situ* RHEED shows the cubic and hexagonal-like transmission RHEED patterns for HOSG(001)-QDs and HOSG(111)-QDs. (c) ω -2θ rocking curve results of MgO(200) peak ($2\theta \approx 42.9^\circ$ marked with *) shows the singular Au-phase ((001) at 44.3° or (111) at 38.1°) while no other Au phases are found. (d) AFM results reveal the squarelike HOSG(001)-QDs aligned along the ⟨110⟩ directions of MgO(001) while HOSG(111)-QDs form hexagonal or triangular shapes. The insets show the lateral size (diameter) distribution of HOSG-QDs. ((i) 650 °C, HOSG(001)-QDs, average size of 27.4 ± 7.7 nm; (ii) 650 °C, HOSG(111)-QDs, average size of 38.2 ± 13.2 nm; (iii) 750 °C: average size of 27.2 ± 6.6 nm.)

ment,^{12,14–18} conversely, can manipulate and generate exotic fundamental properties of low-dimensional materials, that is, when the size of the materials is of the same magnitude as the de Broglie wavelength of the electron wave function. For this reason, low-dimensional materials would have different properties than its three-dimensional bulk counterparts. Nanostructured-Au, for instance, has different physical and chemical properties from bulk-Au. Besides being chemically active,^{16,19} its optical and electrical responses to photons also change. Notably, there has been a lot of research effort on using colloidal Au-nanoparticles for plasmonic sensors, electronics, and biomedical applications^{18,20–23} due to their tunable optical properties with the emergence of surface plasmon resonance in the visible-range. However, all of these nanoparticles were not pure gold but instead required some

complex polymer coating, and the plasmonic properties that were observed were conventional charge plasmons³ associated with oscillations of free electrons in the assembly of Au-nanoparticles. Another problem is the low reproducibility due to the complexity of the assembly Au nanoparticles, which make it difficult to control the conventional charge plasmons and its optical properties.

Herein, a novel class of a strongly correlated-plasmonic material with spin-polarization and orbital-ordering comprising highly oriented single-crystal Au quantum-dots (HOSG-QDs) self-organized on MgO(001) is fabricated with high reproducibility using a unique ultrahigh-vacuum molecular-beam-epitaxy pulsed-laser-deposition (UHV-MBE-PLD) system. In particular, we discover a new unconventional spin plasmon, namely spin correlated-plasmon, and quantum absorption state

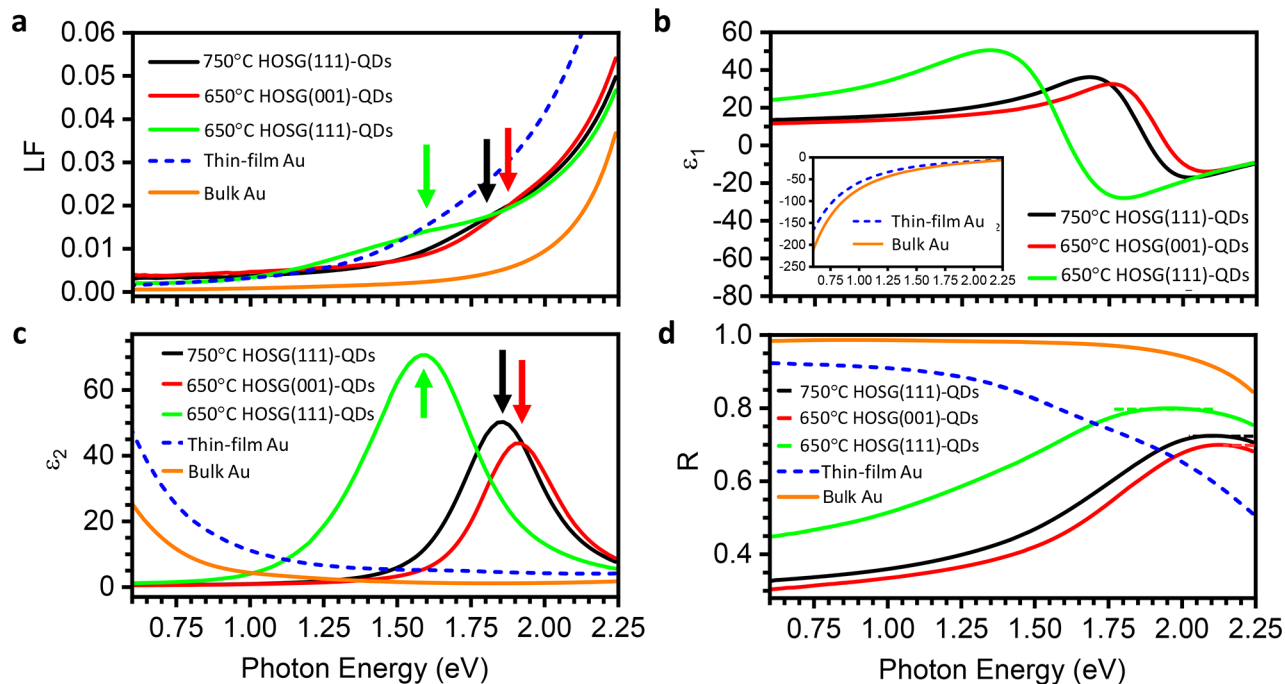


Figure 2. Optical responses of HOSG(001)-QDs and HOSG(111)-QDs in comparison to thin-film and bulk Au. (a) Loss-function plots revealing new peaks at 1.54, 1.88, and 1.82 eV formed by 650 °C HOSG(111)-QDs, 650 °C HOSG(001)-QDs, and 750 °C HOSG(111)-QDs, respectively, in contrast to bulk Au. (b) The real part of complex dielectric function (ϵ_1) remains positive while ϵ_2 in (c) shows peaks around 1.58, 1.90, and 1.86 eV for 650 °C HOSG(111)-QDs, 650 °C HOSG(001)-QDs, and 750 °C HOSG(111)-QDs, respectively. Thin film Au resembles closely bulk Au where ϵ_1 is negative at photon energies from 0.5 to 2.25 eV. The ϵ_2 of thin film Au reveals the Drude response similar to bulk Au. (d) HOSG-QDs reveal a decrease in the R below photon energies of 1.9 eV while thin film Au shows the opposite trend where R increases to ~0.9 with decreasing photon energy.

through quantum confinement in HOSG-QDs. By tuning oxygen overpressure and growth temperature, HOSG-QDs with different crystal orientations (either along (001) or (111)//MgO(001)) and sizes are achieved. We perform a comprehensive experimental method of advanced spectroscopic ellipsometry (SE), X-ray absorption spectroscopy (XAS), X-ray magnetic circular dichroism (XMCD), and electron and X-ray diffraction measurements on HOSG-QDs as a function of size and crystal orientations with thin polycrystalline film and bulk Au for references. We also perform detailed theoretical calculations without and with hybridizations and on-site Hubbard repulsion for different size and geometry of QDs to reveal the role of quantum confinement and electronic correlations. For the first time, we demonstrate and find that the sensitivity of spin-polarized correlated-plasmons on SERS is surprisingly very high.

RESULTS AND DISCUSSION

Controlling the growth process, purity, and cleanliness of Au at the nanoscale in real-time during deposition is an essential prerequisite to make exotic HOSG-QDs structures with the desired optical properties for fundamental science and technological applications. For this purpose, a UHV-MBE-PLD system equipped with reflection high energy electron diffraction (RHEED) and electron spectroscopies for surface characterizations is designed and ideally suited for *in situ* probing of the growth mode, crystal ordering, and epitaxy. Using this technique, we demonstrate a clean, simple, and one-step fabrication approach to produce HOSG-QDs reproducibly on MgO(001) substrate. In PLD of Au on MgO(001) above 350 °C, *in situ* RHEED observations (Figure 1b),

together with postgrowth high-resolution synchrotron radiation X-ray diffraction (XRD) MgO-(002) rocking curve analyses (Figure 1c) and atomic force microscopy (Figure 1d) scans of the surface morphologies, reveal a Volmer–Weber epitaxial growth-mode. Two types of HOSG-QD structures are found to be self-organized on the MgO(001) substrate. Specifically, growth in the presence of O₂ leads to preferential and selective formation of square-shaped HOSG(001)-QDs with face-centered cubic Au(001) planes parallel to the MgO(001) substrate. Contrastingly, growth without O₂ results in the formation of hexagonal- and triangular-shaped HOSG(111)-QDs decorating the MgO(001) surface with low surface energy Au(111) planes parallel to the MgO(001) substrate. By growing in an oxygen-rich regime, the cubic-on-cubic growth of square-shaped HOSG-QDs on MgO(001) surface is promoted by preserving the surface registry of the idealized MgO(001) square unit-cell with little or no oxygen vacancies for the stronger Au–O binding.²⁴ Higher-growth temperatures lead to the formation of smaller HOSG-QDs while room-temperature growth results in bulklike Au polycrystalline thin film (see Supporting Information (SI) Note 1).

Formation of self-organized HOSG-QDs and Au thin films can thus be templated on a MgO(001) surface in this one-step fabrication process. It avoids the need for multistep processes and complexity of solution-based methods typically established for the synthesis of colloidal Au-NPs, often involving capping with surfactants for stabilization²⁵ and subsequently performing the Langmuir–Blodgett technique for self-assembly on substrates.^{26,27} The UHV-MBE-PLD with *in situ* RHEED technique provides a direct and real-time control and the

ability to tune the crystallinity, phase, size, and structure of these HOSG-QDs (i.e., either the preferential formation of HOSG(111)-QDs or HOSG(001)-QDs, and/or the coexistence of both types of HOSG-QDs epitaxially on the MgO(001) surface). This is important as it allows for the first time the optical response, quantitatively and qualitatively, from these HOSG-QDs to be studied unambiguously using advanced spectroscopic ellipsometry, which is sensitive to spin and charge excitations.^{28,29} Together with XAS, XMCD, and electron and X-ray diffractions and supported with theoretical calculations, simultaneous and direct measurement of spin, charge, orbital, and lattice of Au on MgO can thus be ascertained to provide insight into its fundamental spin and electronic interactions with photons, either as a regular noble metal and/or as a strongly correlated electron system. Note that the growth system of UHV-MBE-PLD and *in situ* characterizations of RHEED, ARPES, XPS (see SI Note 3), XAS, XMCD, XLD, and reflectance are all integrated in the new soft X-ray-ultraviolet (SUV) beamline of Singapore Synchrotron Light Source and such *in situ* characterizations also ensure unambiguity.³⁰

Au thin film exhibits characteristics of a metallic conducting film akin to bulk Au (Figure 2) as shown in the optical response arising from the loss function, $-\text{Im}[1/\epsilon]$ (Figure 2a), which is the most direct way to measure plasmon response, complex dielectric function, $\epsilon \equiv \epsilon_1 + i\epsilon_2$ (Figure 2b,c), and reflectivity, R (Figure 2d). For photon energies less than 1 eV, ϵ_1 shows a very high negative value, as typical of Au bulk, suggesting that the low energy electrons are screened (inset of Figure 2b). ϵ_2 shows the typical Drude response for Au as a metal arising from the electronic intraband transitions dominated by free-electron behavior in the partially filled sp bands, which cross the Fermi-level (Figure 2c). For photon energies of ~ 1 to ~ 2 eV, ϵ_2 is suppressed and ϵ_1 approaches finite values but remains negative. The loss function exhibits an associated absorption tail of interband contributions ($5d \rightarrow 6sp$), which extends to about 1.8 eV (Figure 2a).

Our main observation is that HOSG-QDs remarkably show a vastly different optical response. The loss function now has new peaks at about 1.54, 1.88, and 1.82 eV for 650 °C HOSG(111)-QDs, 650 °C HOSG(001)-QDs, and 750 °C HOSG(111)-QDs, respectively (Figure 2a). Through a thoroughly and comprehensive analysis supported with detailed theoretical calculations (as presented below), these peaks are attributed to the presence of a new exotic unconventional plasmon, namely spin correlated-plasmon, arising from surprisingly strong spin-polarization s band of HOSG-QDs self-organized on MgO(001). They are also distinctively missing from the optical response for the Au thin film and bulk Au. For photon energies less than 1 eV, interestingly, ϵ_1 turns positive (Figure 2b) revealing that electrons are unusually unscreened. More significantly, ϵ_2 shows spectral weight transfer in a broad energy range, that is, a dramatic suppression of the low-energy Drude response accompanied by an occurrence of an anomalous quantum absorption of a midgap state at ~ 1.58 , ~ 1.90 , and ~ 1.86 eV for 650 °C HOSG(111)-QDs, 650 °C HOSG(001)-QDs, and 750 °C HOSG(111)-QDs, respectively (Figure 2c). The quantum absorption occurs due to unusually strong spin-polarization in Au-6s and hybridizations of Au-6sp with 5d bands, and its energy determining the strength of the spin-splitting. The intensity of ϵ_2 of quantum absorption is enormous, which is as high as ~ 70 . While ϵ_1 is unusually high approaching ~ 50 . This

spectral weight transfer is a fingerprint of strong electronic correlations, responsible for generating metal to Mott-like insulator transition and transparency and yielding the new spin correlated-plasmon observed in the loss function of HOSG-QDs (Figure 2a). The energy of spectral weight transfer observed in HOSG-QDs is surprisingly large, that is, at least ~ 1.58 eV, a magnitude that is comparable to the strong electron-electron correlations³¹ in the charge transfer (O2p–Cu3d) of copper oxide-based high-temperature superconductors (cuprates)³² and in d-d Mott-transition of manganites as revealed by high-energy optical conductivity measurements.¹¹ This is unusual because electrons in s band are well-screened and noncorrelated as shown in the bulk Au as well as Au thin film. Such strong electron-electron correlations in s band of HOSG-QDs create a Mott-like gap, which is comparable to the direct bandgap of semiconductors such as GaAs whose E_g is about 1.4 eV.³³ The peak position is found to shift to higher energies as the QD size decreases. The differences in optical response are also revealed in the reflectivity plots of Figure 2d, where a significant decrease in reflectivity around photon energies of 1.9 and 2.0 eV occurs for HOSG-QDs but not for bulklike thin film.

These unusual optical responses, attributed to the presence of the spin correlated-plasmon in HOSG-QDs, are due to spin-polarization bands as proven in our XAS and XMCD measurements (Figure 3) supported with theoretical calculations (Figure 3; also see SI Note 2). Particularly, we find that the degeneracy of the 6s bands at the Fermi-level is lifted and split to form a gap between the spin-up and spin-down states. Indeed, XAS measurements at room temperature (Figure 3a) show unequivocally the existence of a new Au 6s+5d

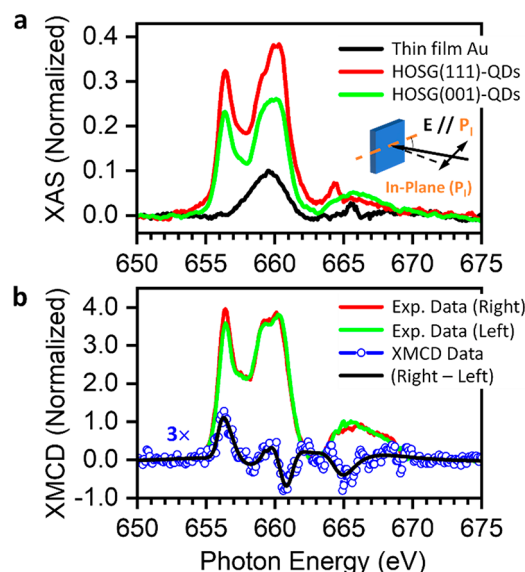


Figure 3. XAS and XMCD spectra of HOSG(001)-QDs and HOSG(111)-QDs. (a) XAS spectra of HOSG(111)-QDs and HOSG(001)-QDs taken where E-field of the incident photon is parallel to the MgO(001) substrate in-plane axis (P_1) respectively. The spectra show strongly enhanced, well-resolved peaks due to quantum confinement effects along with the formation of hybridized $6sp+5d$ state at 656 eV, which is not seen in thin film Au. The broad hump at 660 eV for thin film Au depicts the $Au4p \rightarrow 6sp$ transition. (b) XMCD spectra of HOSG(111)-QDs using left and right circular polarized lights, taken at room temperature without applied external magnetic field, reveal strong spin-states at 656, 651, and 665 eV.

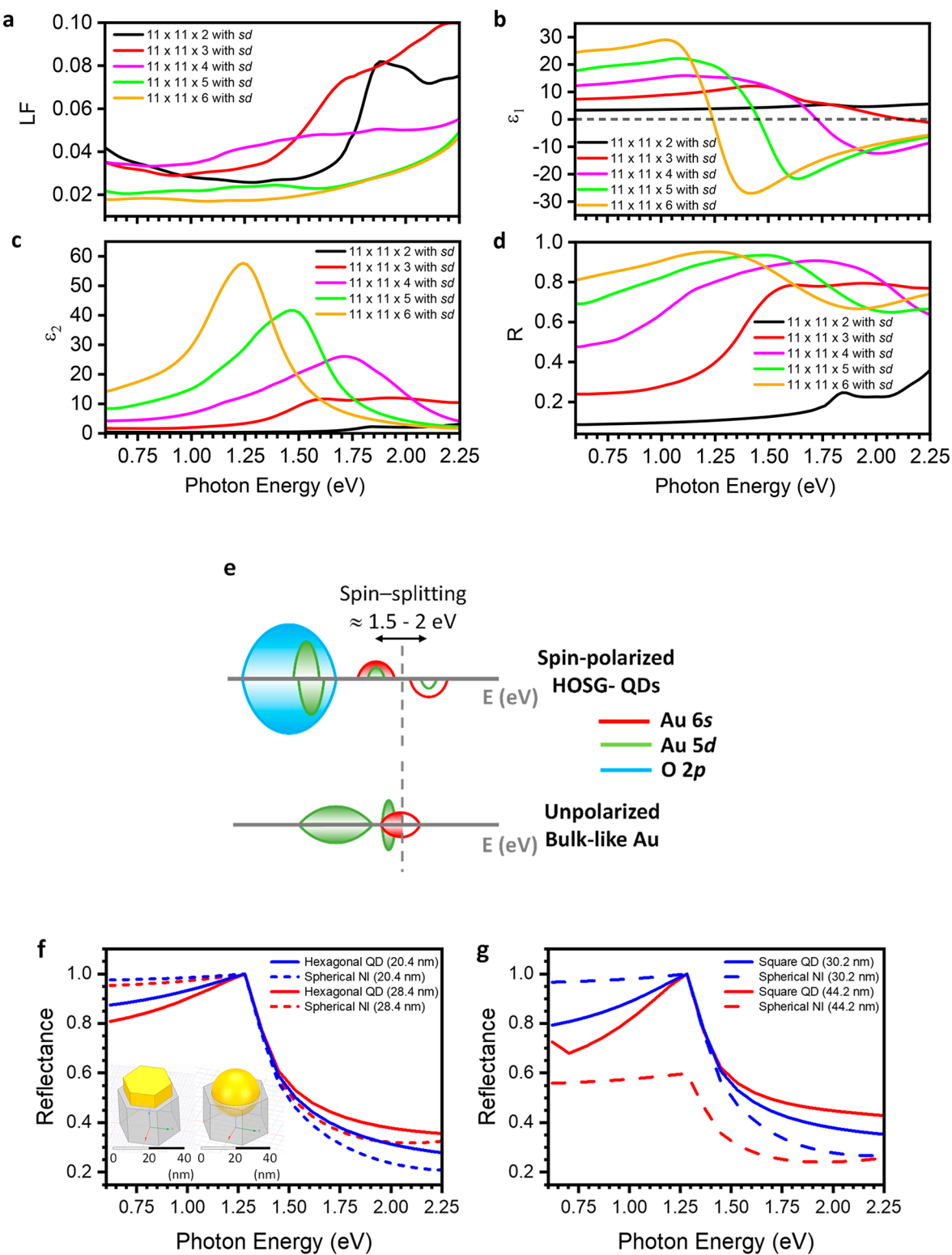


Figure 4. Theoretical calculation and modeling of Au on MgO(001). (a-d) Optical responses showing the effect of thickness variation on the out-of-plane optical responses with s-d hybridization, $V_{s-d} = 1$ eV, for Au systems with size $11 \times 11 \times N$ atoms (where $N = 2, 3, 4, 5$ or 6). (e) Schematic band energy diagrams depicting the spin-polarized, spin-splitting, and hybridization of 6s-5d density-of-states near the Fermi-level for HOSG-QDs, in contrast to unpolarized bulklike Au. (f) FDTD electromagnetic simulation results showing calculated reflectivity from an infinite array of hexagonal-shaped quantum dots (QD) and partially embedded spherical nanoislands (NI). The diameter is set at 20.4 nm (blue lines) and 28.4 nm (red lines). Both systems are arranged in a hexagonal array with a spacing of 7 nm between the QD or NI. Inset: Geometries of a single hexagonal QD and a single spherical NI. (g) FDTD simulation shows the calculated reflectivity from an infinite array of square-shaped QD and partially embedded spherical NI. The diameter is set at 30.2 nm (blue lines) and 44.2 nm (red lines). Both systems are arranged in a square array with a spacing of 7 nm between the QD or NI. The simulations are run with QD (or NI) sizes in the same range as the hexagonal-shaped HOSG-QDs and square-shaped HOSG-QDs shown in Figure 1.

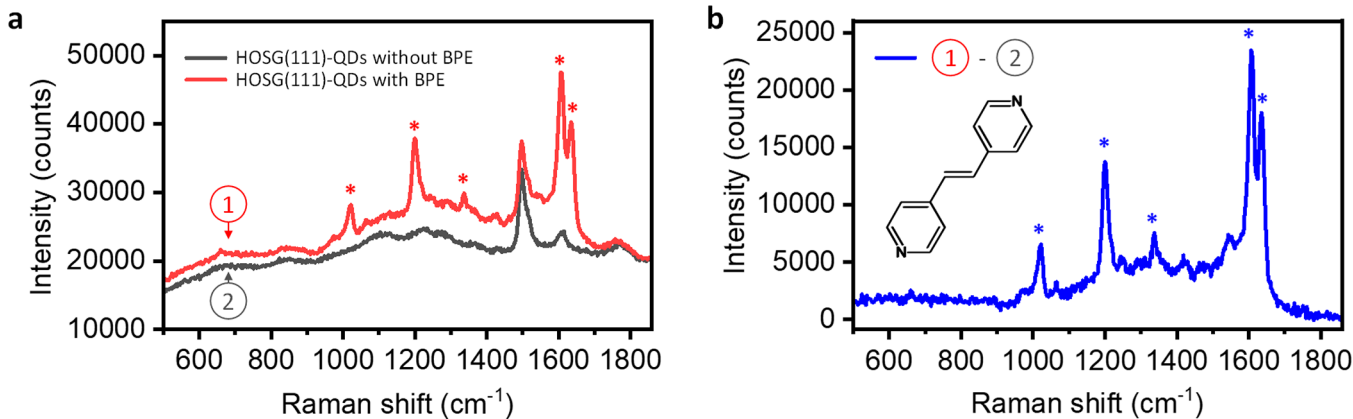


Figure 5. SERS spectra of BPE on HOSG(111)-QDs. (a) Raman spectrum of BPE ($10 \mu\text{M}$, 1.82 ppm) molecule dropped and dried on the HOSG(111)-QDs. Compared with the Raman spectrum without BPE analyte (black), the HOSG(111)-QDs with BPE analyte (red) shows additional peaks. The strong Raman signals (marked with *) after background subtraction shown in (b) are major BPE Raman peaks.

hybridization state yielding $\text{Au } 4p \rightarrow 6s+5d$ transition at $\sim 656 \text{ eV}$, which is absent in the bulk thin film. For the bulklike thin film Au, only a broad hump at $\sim 660 \text{ eV}$ attributed to the $\text{Au } 4p \rightarrow 6sp$ transition is observed. For the HOSG-QDs, intriguingly, a new sharp peak at $\sim 656 \text{ eV}$ is observed, while the peak at $\sim 660 \text{ eV}$ becomes enhanced and well-resolved into multiple peaks (Figure 3a). This new sharp peak at $\sim 656 \text{ eV}$ is attributed to the interplay between electron–electron interactions, quantum confinement due to size and orientation and Au-6s hybridized with 5d through the O2p state arising from the self-assembly of HOSG-QDs on $\text{MgO}(001)$ yielding to spin-polarized bands as supported by previous density functional theory calculations.²⁴

Interestingly, room-temperature XMCD measurements, which are acquired intentionally without magnetic field, directly reveal strong signal of ferromagnetism, spin-polarization, and ordering as shown in Figure 3b. The XMCD signal is the strongest at the new $\sim 656 \text{ eV}$ peak of $\text{Au-4p} \rightarrow 6s+5d$ transition, revealing the strong spin-polarization of Au-6s. While the energy separation between the strongest XMCD peak with the next XMCD dip (or negative peak) is about $1.5\text{--}2 \text{ eV}$, uncovering strong spin-splitting. These are all consistent with SE measurements. Furthermore, XMCD measurements further reveal that these well-resolved new peaks at higher energy around 660 eV are also spin-polarized. It is worth noting that the spin ordering is a signature of strongly correlated electron systems, which are known to occur in high-temperature superconducting cuprates and manganese-systems and may determine the Mott gaplike states.^{34–36} In HOSG-QDs, the large Mott gaplike state ($>1.5 \text{ eV}$) is consistent with these strongly correlated-electron systems.

Our experimental observations are supported by theoretical calculations. Using a tight-binding model incorporating s–d hybridizations and on-site Hubbard repulsion treated within mean field approximation, our theoretical calculations show that the occurrence of the unconventional spin correlated-plasmon is due to the existence of strong electronic correlations; in this case, the s–d hybridization and hopping electrons due to the finite sizes of Au quantum dot formation on $\text{MgO}(001)$ (see SI Note 2). The presence of s–d hybridization creates splitting in the partial density of states for both s and d bands (Figure S2). The calculated out-of-plane optical responses of LF, ϵ_1 , ϵ_2 , and reflectivity agree well with our experimental results (Figures 4a–d). The calculated

LF indeed shows spin correlated-plasmon in the visible accompanied by positive value of ϵ_1 . A new Mott-like gap state is also captured in our calculated ϵ_2 . Suppression low-energy Drude response is shown in the calculated ϵ_2 accompanied by a positive and high value of the calculated ϵ_1 . From our theoretical calculations, we also infer that the optical response data have a dominant contribution from the out-of-plane responses. Combining both experimental data and our theoretical calculations, we propose new electronic structure of HOSG-QDs (Figure 4e). It is found that an interplay of electron–electron correlations, s–d hybridization, and quantum confinement in the HOSG-QDs plays an important role in the generation of the spin-correlated-plasmon in the loss function, a quantum absorption Mott-like state, and disappearance of low-energy Drude response in complex dielectric functions (see SI Note 2). Such an interplay changes the Au-6s degenerate state to a split spin-polarized state with an energy difference of about $1.5\text{--}2 \text{ eV}$ between the split states (Figure 4b,e) as identified by the quantum absorption (Figure 2c).

For comparison, we also perform electromagnetic calculations based on finite difference time domain (FDTD) and calculate the optical reflectivity based on different quantum dot shapes and sizes of HOSG-QDs but without electronic correlations (Figure 4f,g). We find that the quantum confinement due to the shapes and sizes alone cannot explain our experimental results (c.f. Figure 2d). This further supports that electronic correlations are enhanced and play an important role (Figure 4) in the quantum confinement of HOSG-QDs.

A direct and useful technological application of this unique spin correlated-plasmon's property is demonstrated using HOSG-QDs as a SERS-chip, that is, Spin-SERS, with 1,2-di(4-pyridyl)ethylene (BPE) as the analyte (see SI Note 4 and ref 37). Intriguingly, strong SERS signals (Figure 5) are observed when $10 \mu\text{M}$ (1.8 ppm) of BPE dripped and dried on the Spin-SERS chip was excited using laser with photon energy of 633 nm ($\sim 1.96 \text{ eV}$), which is resonant at the spin correlated-plasmon. We observe Raman peaks at (i) 1020 cm^{-1} due to (C–N) and (C–C) stretching modes, (ii) 1200 cm^{-1} due to (C_r–C_b) stretching and rocking modes where C_r is a ring-carbon bonded to a bridging carbon and C_b is a bridging-carbon,³⁸ (iii) 1335 cm^{-1} due to (C=C) bending modes, and last (iv) 1607 and 1635 cm^{-1} , which are BPE characteristic

peaks due to (C–C) stretching modes.³⁹ In contrast, no SERS signal is observed using SERS-substrate of Au thin film or quartz slide with the same analyte further signifying the unique role of the spin correlated-plasmon generated in HOSG-QDs and not in continuous Au thin film (Figure S7). To further support the high sensitivity of Spin-SERS method, we are able to acquire about 23 000 counts (based on the 1607 cm⁻¹ peak for a 1.8 ppm analyte) within a 3 s integration time and 11 mW laser. It is worthwhile to mention that since currently available SERS-active substrates have fundamental challenges of either being not reproducible or very complex and difficult to prepare,⁴⁰ the spin correlated-plasmon in HOSG-QDs can address and overcome them. The spin correlated-plasmon, a quantum oscillation of an interplay of spin and charge due to electronic correlations in strongly correlated electron systems, opens new fundamental science and applications such as combined spintronic–plasmonic applications.¹⁷

CONCLUSION

In conclusion, we present a novel class of strongly correlated, Mott-like insulating gold in the form of highly oriented single-crystalline gold quantum-dots (HOSG-QDs) grown on MgO using MBE-PLD. Intriguingly, by controlling quantum confinement, that is, the size and orientation of the HOSG-QDs, electronic correlations are enhanced yielding a new room-temperature spin correlated-plasmon and a quantum absorption Mott-like state, which are all tunable from the infrared to visible. We find unusually strong spin-polarization and spin-splitting (~1.5–2 eV) of Au-6s and hybridizations of Au-6s with Au-5d yielding ferromagnetism in s band of gold. The first demonstration of the spin correlated-plasmons with a very high sensitivity in the surface-enhanced Raman spectroscopy is also presented. Our result shows the importance of the interplay between the spin, charge, and quantum confinement in determining electronic structure and correlations of novel correlated material, Mott-like insulating HOSG-QDs and opens new, great potential for spintronic–plasmonic applications.

ASSOCIATED CONTENT

Supporting Information

The Supporting Information is available free of charge at <https://pubs.acs.org/doi/10.1021/acs.nanolett.0c05004>.

Materials and Methods; Supporting notes 1–5; Figures S1–S9 (PDF)

AUTHOR INFORMATION

Corresponding Author

Andriyo Rusydi – Advanced Research Initiative for Correlated-Electron Systems (ARiCES), Department of Physics, National University of Singapore, Singapore 117551, Singapore; Present Address: Advanced Research Initiative for Correlated-Electron Systems (ARiCES), Department of Physics, National University of Singapore, 2 Science Drive 3, Singapore 117551, Singapore; Present Address: Singapore Synchrotron Light Source, 5 Research Link, Singapore 117603, Singapore.; Present Address: NUSNNI-NanoCore, National University of Singapore, Singapore 117411.; Email: andriyo.rusydi@nus.edu.sg

Authors

Bin Leong Ong – Advanced Research Initiative for Correlated-Electron Systems (ARiCES), Department of Physics, National University of Singapore, Singapore 117551, Singapore; Present Address: Advanced Research Initiative for Correlated-Electron Systems (ARiCES), Department of Physics, National University of Singapore, 2 Science Drive 3, Singapore 117551, Singapore; orcid.org/0000-0002-3438-7616

Muhammad Avicenna Naradipa – Advanced Research Initiative for Correlated-Electron Systems (ARiCES), Department of Physics, National University of Singapore, Singapore 117551, Singapore; Present Address: Advanced Research Initiative for Correlated-Electron Systems (ARiCES), Department of Physics, National University of Singapore, 2 Science Drive 3, Singapore 117551, Singapore; orcid.org/0000-0003-4210-6789

Angga Dito Fauzi – Advanced Research Initiative for Correlated-Electron Systems (ARiCES), Department of Physics, National University of Singapore, Singapore 117551, Singapore; Present Address: Advanced Research Initiative for Correlated-Electron Systems (ARiCES), Department of Physics, National University of Singapore, 2 Science Drive 3, Singapore 117551, Singapore

Muhammad Aziz Majidi – Advanced Research Initiative for Correlated-Electron Systems (ARiCES), Department of Physics, National University of Singapore, Singapore 117551, Singapore; Present Address: Department of Physics, FMIPA, Universitas Indonesia, Depok 16424, Indonesia.

Caozheng Diao – Advanced Research Initiative for Correlated-Electron Systems (ARiCES), Department of Physics, National University of Singapore, Singapore 117551, Singapore; Present Address: Singapore Synchrotron Light Source, 5 Research Link, Singapore 117603, Singapore.

Satoshi Kurumi – Advanced Research Initiative for Correlated-Electron Systems (ARiCES), Department of Physics, National University of Singapore, Singapore 117551, Singapore; Present Address: College of Science and Technology, Nihon University, 1-8-14 Kanda-Surugadai, Chiyoda-ku, Tokyo 101–8308, Japan.

Pranab Kumar Das – Advanced Research Initiative for Correlated-Electron Systems (ARiCES), Department of Physics, National University of Singapore, Singapore 117551, Singapore; Present Address: Singapore Synchrotron Light Source, 5 Research Link, Singapore 117603, Singapore.

Chi Xiao – Advanced Research Initiative for Correlated-Electron Systems (ARiCES), Department of Physics, National University of Singapore, Singapore 117551, Singapore; Present Address: Singapore Synchrotron Light Source, 5 Research Link, Singapore 117603, Singapore.

Ping Yang – Advanced Research Initiative for Correlated-Electron Systems (ARiCES), Department of Physics, National University of Singapore, Singapore 117551, Singapore; Present Address: Singapore Synchrotron Light Source, 5 Research Link, Singapore 117603, Singapore.

Mark B. H. Breese – Advanced Research Initiative for Correlated-Electron Systems (ARiCES), Department of Physics, National University of Singapore, Singapore 117551, Singapore; Present Address: Singapore Synchrotron Light Source, 5 Research Link, Singapore 117603, Singapore.

Sheau Wei Ong – Advanced Research Initiative for Correlated-Electron Systems (ARiCES), Department of Physics, National University of Singapore, Singapore 117551,

Singapore; Present Address: Advanced Research Initiative for Correlated-Electron Systems (ARiCES), Department of Physics, National University of Singapore, 2 Science Drive 3, Singapore 117551, Singapore

Khay Ming Tan — Advanced Research Initiative for Correlated-Electron Systems (ARiCES), Department of Physics, National University of Singapore, Singapore 117551, Singapore; Present Address: TechnoSpex Pte. Ltd., 1092 Lower Delta Rd, #04–01, Singapore 169203, Singapore.

Eng Soon Tok — Advanced Research Initiative for Correlated-Electron Systems (ARiCES), Department of Physics, National University of Singapore, Singapore 117551, Singapore; Present Address: Advanced Research Initiative for Correlated-Electron Systems (ARiCES), Department of Physics, National University of Singapore, 2 Science Drive 3, Singapore 117551, Singapore

Complete contact information is available at:

<https://pubs.acs.org/10.1021/acs.nanolett.0c05004>

Author Contributions

B.L.O., E.S.T., and A.R., assisted by S.K., grew samples and performed RHEED and AFM measurements. M.A.N., and A.R. performed spectroscopic ellipsometry measurements. A.D.F., C.D., and A.R. performed XAS, XMCD, and XLD measurements. P.K.D., B.L.O., and A.R. performed XPS measurements. B.L.O., C.X., P.Y., S.W.O., E.S.T., and A.R. performed XRD measurements. M.A.M. and A.R. performed theoretical calculations. K.M.T., E.S.T., and A.R. performed SERS measurements. B.L.O., E.S.T., and A.R. analyzed data comprehensively and wrote the manuscript with inputs from all coauthors. A.R. designed the integrated UHV-MBE-PLD with *in situ* RHEED, XAS, XMCD, XLD, and reflectance and led the project.

Funding

This work was supported by the Ministry of Education of Singapore (MOE) AcRF Tier-2 (MOE2017-T2-1-135, MOE2018-T2-2-117, and MOE2019-T2-1-163), MOE AcRF Tier-1 (R-144-000-423-114, R-144-000-398-114, and R-144-000-439-114), NUS Core Support (C-380-003-003-001), and the Singapore National Research Foundation under its Competitive Research Funding (No. NRF-CRP 8-2011-06 and No. R-398-000-087-281).

Notes

The authors declare no competing financial interest.

ACKNOWLEDGMENTS

The authors thank Jason Chee Wai Lim for technical supports and Singapore Synchrotron Light Source (SSLS) for providing the facility necessary for conducting the research. SSLS is a National Research Infrastructure under the Singapore National Research Foundation.

REFERENCES

- (1) Mott, N. F. The Basis of the Electron Theory of Metals, with Special Reference to the Transition Metals. *Proc. Phys. Soc., London, Sect. A* **1949**, *62* (7), 416–422.
- (2) Mott, N. F. Electrons in Transition Metals. *Adv. Phys.* **1964**, *13* (51), 325–422.
- (3) Pines, D.; Bohm, D. A Collective Description of Electron Interactions: II. Collective vs Individual Particle Aspects of the Interactions. *Phys. Rev.* **1952**, *85* (2), 338–353.

(4) Agarwal, A.; Polini, M.; Vignale, G.; Flatté, M. E. Long-Lived Spin Plasmons in a Spin-Polarized Two-Dimensional Electron Gas. *Phys. Rev. B: Condens. Matter Mater. Phys.* **2014**, *90* (15), 155409.

(5) Agarwal, A.; Vignale, G. Plasmons in Spin-Polarized Graphene: A Way to Measure Spin Polarization. *Phys. Rev. B: Condens. Matter Mater. Phys.* **2015**, *91* (24), 245407.

(6) Maier, S. A. *Plasmonics: Fundamentals and Applications*; Springer Science and Business Media: New York, 2007.

(7) van Loon, E. G. C. P.; Hafermann, H.; Lichtenstein, A. I.; Rubtsov, A. N.; Katsnelson, M. I. Plasmons in Strongly Correlated Systems: Spectral Weight Transfer and Renormalized Dispersion. *Phys. Rev. Lett.* **2014**, *113* (24), 246407.

(8) Hubbard, J.; Flowers, B. H. Electron Correlations in Narrow Energy Bands V. A Perturbation Expansion about the Atomic Limit. *Proc. R. Soc. London. Ser. A. Math. Phys. Sci.* **1967**, *296* (1444), 82–99.

(9) Eskes, H.; Meinders, M. B. J.; Sawatzky, G. A. Anomalous Transfer of Spectral Weight in Doped Strongly Correlated Systems. *Phys. Rev. Lett.* **1991**, *67* (8), 1035–1038.

(10) Ohta, Y.; Tsutsui, K.; Koshiba, W.; Shimozato, T.; Maekawa, S. Evolution of the In-Gap State in High-T_c Cuprates. *Phys. Rev. B: Condens. Matter Mater. Phys.* **1992**, *46* (21), 14022–14033.

(11) Rusydi, A.; Rauer, R.; Neuber, G.; Bastjan, M.; Mahns, I.; Müller, S.; Saichu, P.; Schulz, B.; Singer, S. G.; Lichtenstein, A. I.; Qi, D.; Gao, X.; Yu, X.; Wee, A. T. S.; Stryganyuk, G.; Dörr, K.; Sawatzky, G. A.; Cooper, S. L.; Rübhausen, M. Metal-Insulator Transition in Manganites: Changes in Optical Conductivity up to 22 EV. *Phys. Rev. B: Condens. Matter Mater. Phys.* **2008**, *78* (12), 125110.

(12) Asmara, T. C.; Wan, D.; Zhao, Y.; Majidi, M. A.; Nelson, C. T.; Scott, M. C.; Cai, Y.; Yan, B.; Schmidt, D.; Yang, M.; Zhu, T.; Trevisanutto, P. E.; Motapothula, M. R.; Feng, Y. P.; Breese, M. B. H.; Sherburne, M.; Asta, M.; Minor, A.; Venkatesan, T.; Rusydi, A. Tunable and Low-Loss Correlated Plasmons in Mott-like Insulating Oxides. *Nat. Commun.* **2017**, *8* (March), 1–11.

(13) Hammer, B.; Norskov, J. K. Why Gold Is the Noblest of All the Metals. *Nature* **1995**, *376* (6537), 238–240.

(14) Haug, H.; Koch, S. W. *Quantum Theory of the Optical and Electronic Properties of Semiconductors*, third ed.; World Scientific: Singapore, 1994.

(15) Wilson, W. L.; Szajowski, P. F.; Brus, L. E. Quantum Confinement in Size-Selected, Surface-Oxidized Silicon Nanocrystals. *Science* **1993**, *262* (5137), 1242–1244.

(16) Hughes, M. D.; Xu, Y. J.; Jenkins, P.; McMorn, P.; Landon, P.; Enache, D. I.; Carley, A. F.; Attard, G. A.; Hutchings, G. J.; King, F.; Stitt, E. H.; Johnston, P.; Griffin, K.; Kiely, C. J. Tunable Gold Catalysts for Selective Hydrocarbon Oxidation under Mild Conditions. *Nature* **2005**, *437* (7062), 1132–1135.

(17) Temnov, V. V.; Armelles, G.; Woggon, U.; Guzatov, D.; Cebollada, A.; Garcia-Martin, A.; Garcia-Martin, J. M.; Thomay, T.; Leitenstorfer, A.; Bratschitsch, R. Active Magneto-Plasmonics in Hybrid Metal-Ferromagnet Structures. *Nat. Photonics* **2010**, *4* (2), 107–111.

(18) Cho, E. S.; Kim, J.; Tejerina, B.; Hermans, T. M.; Jiang, H.; Nakanishi, H.; Yu, M.; Patashinski, A. Z.; Glotzer, S. C.; Stellacci, F.; Grzybowski, B. A. Ultrasensitive Detection of Toxic Cations through Changes in the Tunnelling Current across Films of Striped Nanoparticles. *Nat. Mater.* **2012**, *11* (11), 978–985.

(19) Sinha, A. K.; Seelan, S.; Tsubota, S.; Haruta, M. A Three-Dimensional Mesoporous Titanosilicate Support for Gold Nanoparticles: Vapor-Phase Epoxidation of Propene with High Conversion. *Angew. Chem., Int. Ed.* **2004**, *43* (12), 1546–1548.

(20) Ahmed, S. R.; Kim, J.; Tran, V. T.; Suzuki, T.; Neethirajan, S.; Lee, J.; Park, E. Y. In Situ Self-Assembly of Gold Nanoparticles on Hydrophilic and Hydrophobic Substrates for Influenza Virus-Sensing Platform. *Sci. Rep.* **2017**, *7* (1), 1–11.

(21) Ghosh, P.; Han, G.; De, M.; Kim, C. K.; Rotello, V. M. Gold Nanoparticles in Delivery Applications. *Adv. Drug Delivery Rev.* **2008**, *60* (11), 1307–1315.

- (22) Anker, J. N.; Hall, W. P.; Lyandres, O.; Shah, N. C.; Zhao, J.; Van Duyne, R. P. Biosensing with Plasmonic Nanosensors. *Nat. Mater.* **2008**, *7* (6), 442–453.
- (23) Cecconello, A.; Besteiro, L. V.; Govorov, A. O.; Willner, I. Chiroplasmonic DNA-Based Nanostructures. *Nat. Rev. Mater.* **2017**, *2* (9), 17039.
- (24) Giordano, L.; Baistrocchi, M.; Pacchioni, G. Bonding of Pd, Ag, and Au Atoms on MgO(100) Surfaces and MgO/Mo(100) Ultra-Thin Films: A Comparative DFT Study. *Phys. Rev. B: Condens. Matter Mater. Phys.* **2005**, *72* (11), 1–11.
- (25) Daniel, M.-C.; Astruc, D. Gold Nanoparticles: Assembly, Supramolecular Chemistry, Quantum-Size-Related Properties, and Applications toward Biology, Catalysis, and Nanotechnology. *Chem. Rev.* **2004**, *104* (1), 293–346.
- (26) Dong, Y. C.; Hajfathalian, M.; Maidment, P. S. N.; Hsu, J. C.; Naha, P. C.; Si-Mohamed, S.; Breuilly, M.; Kim, J.; Chhour, P.; Douek, P.; Litt, H. I.; Cormode, D. P. Effect of Gold Nanoparticle Size on Their Properties as Contrast Agents for Computed Tomography. *Sci. Rep.* **2019**, *9* (1), 14912.
- (27) Paul, S.; Pearson, C.; Molloy, A.; Cousins, M. A.; Green, M.; Koliopoulou, S.; Dimitrakis, P.; Normand, P.; Tsoukalas, D.; Petty, M. C. Langmuir-Blodgett Film Deposition of Metallic Nanoparticles and Their Application to Electronic Memory Structures. *Nano Lett.* **2003**, *3* (4), 533–536.
- (28) Santoso, I.; Ku, W.; Shirakawa, T.; Neuber, G.; Yin, X.; Enoki, M.; Fujita, M.; Liang, R.; Venkatesan, T.; Sawatzky, G. A.; Kotlov, A.; Yunoki, S.; Rüthausen, M.; Rusydi, A. Unraveling Local Spin Polarization of Zhang-Rice Singlet in Lightly Hole-Doped Cuprates Using High-Energy Optical Conductivity. *Phys. Rev. B: Condens. Matter Mater. Phys.* **2017**, *95* (16), 1–13.
- (29) Fujiwara, H. *Spectroscopic Ellipsometry: Principles and Applications*; Wiley: West Sussex, 2007.
- (30) Yu, X. J.; Diao, C. Z.; Venkatesan, T.; Breese, M. B. H.; Rusydi, A. A Soft X-Ray-Ultraviolet (SUV) Beamline and Diffractometer for Resonant Elastic Scattering and Ultraviolet-Vacuum Ultraviolet Reflectance at the Singapore Synchrotron Light Source. *Rev. Sci. Instrum.* **2018**, *89* (11), 113113.
- (31) Zaanen, J.; Sawatzky, G. A.; Allen, J. W. Band Gaps and Electronic Structure of Transition-Metal Compounds. *Phys. Rev. Lett.* **1985**, *55* (4), 418–421.
- (32) Uchida, S.; Ido, T.; Takagi, H.; Arima, T.; Tokura, Y.; Tajima, S. Optical Spectra of La₂-XS_xCuO₄: Effect of Carrier Doping on the Electronic Structure of the CuO₂ Plane. *Phys. Rev. B: Condens. Matter Mater. Phys.* **1991**, *43* (10), 7942–7954.
- (33) Shur, M. *GaAs Devices and Circuits*, first ed.; Plenum Press: New York, 1987.
- (34) Yin, X.; Zeng, S.; Das, T.; Baskaran, G.; Asmara, T. C.; Santoso, I.; Yu, X.; Diao, C.; Yang, P.; Breese, M. B. H.; Venkatesan, T.; Lin, H.; Ariando; Rusydi, A. Coexistence of Midgap Antiferromagnetic and Mott States in Undoped, Hole- and Electron-Doped Ambipolar Cuprates. *Phys. Rev. Lett.* **2016**, *116* (19), 1–6.
- (35) Kugel, K. I.; Khomskii, D. I. The Jahn-Teller Effect and Magnetism: Transition Metal Compounds. *Sov. Phys. - Uspekhi* **1982**, *25* (4), 231.
- (36) Basov, D. N.; Averitt, R. D.; Van Der Marel, D.; Dressel, M.; Haule, K. Electrodynamics of Correlated Electron Materials. *Rev. Mod. Phys.* **2011**, *83* (2), 471–541.
- (37) Lombardi, J. R.; Birke, R. L. A Unified View of Surface-Enhanced Raman Scattering. *Acc. Chem. Res.* **2009**, *42* (6), 734–742.
- (38) Gao, J.; Qian, H.; Xu, S.; Han, M. Investigation of 1D Silver Nanoparticle Arrays for Use as Molecule Concentration-Specific SERS Substrates. *J. Nanomater.* **2013**, *2013*, 1.
- (39) Péron, O.; Rinnert, E.; Colas, F.; Lehaitre, M.; Compère, C. First Steps of in Situ Surface-Enhanced Raman Scattering during Shipboard Experiments. *Appl. Spectrosc.* **2010**, *64* (10), 1086–1093.
- (40) Yuan, Y.; Panwar, N.; Yap, S. H. K.; Wu, Q.; Zeng, S.; Xu, J.; Tjin, S. C.; Song, J.; Qu, J.; Yong, K.-T. SERS-Based Ultrasensitive Sensing Platform: An Insight into Design and Practical Applications. *Coord. Chem. Rev.* **2017**, *337*, 1–33.